



## Elevated 3D structures of PM<sub>2.5</sub> and impact of complex terrain-forcing circulations on heavy haze pollution over Sichuan Basin, China

Zhuozhi Shu<sup>1,4</sup>, Yubao Liu<sup>1,4</sup>, Tianliang Zhao<sup>1,4,\*</sup>, Junrong Xia<sup>1</sup>, Chenggang Wang<sup>1</sup>, Le  
5 Cao<sup>1</sup>, Haoliang Wang<sup>1</sup>, Lei Zhang<sup>2</sup>, Yu Zheng<sup>2</sup>, Lijuan Shen<sup>1</sup>, Lei Luo<sup>3</sup>, Yueqing Li<sup>3</sup>

<sup>1</sup>Collaborative Innovation Center on Forecast and Evaluation of Meteorological Disasters, Key  
Laboratory for Aerosol-Cloud-Precipitation of China Meteorological Administration, Nanjing  
University of Information Science and Technology, Nanjing, 210044, China

10 <sup>2</sup>State Key Laboratory of Disastrous Weather, China Academy of Meteorological Sciences, Beijing,  
100081, China

<sup>3</sup>Institute of Plateau Meteorology, China Meteorological Administration, Chengdu, 610072, China

<sup>4</sup>Precision Regional Earth Modeling and Information Center, Nanjing University of Information Science  
and Technology, Nanjing, 210044, China

15 *Correspondence:* Tianliang Zhao (tlzhao@nuist.edu.cn)

**Abstract.** Deep basins create a uniquely favorable condition for the formation of air pollution, and the  
Sichuan Basin (SCB) in Southwest China is such a basin featuring frequent heavy pollution. A wintertime  
heavy haze pollution event in SCB was studied with conventional and intensive observation data and the  
WRF-chem model to explore the three-dimensional distribution of PM<sub>2.5</sub> for understanding the impact  
20 of regional pollutant emissions, basin circulations associated with plateaus, and downwind transport to  
the adjacent areas. It was found that the vertical structure of PM<sub>2.5</sub> over SCB was characterized with a  
remarkable hollow sandwiched by high PM<sub>2.5</sub> layers at heights of 1.5–3 km and the highly polluted near-  
surface layer. The southwesterlies passed over the Tibetan Plateau (TP) and Yunan-Guizhou Plateau  
(YGP) resulted in a lee vortex over SCB, which helped form and maintain heavy PM<sub>2.5</sub> pollution. The  
25 basin PM<sub>2.5</sub> was lifted into the free troposphere and transported outside of SCB. At the bottom of SCB,  
high PM<sub>2.5</sub> concentrations were mostly located in the northwest and southern regions. Due to the blocking  
effect of the plateau terrain on the northeasterly winds, PM<sub>2.5</sub> gradually increased from northeast to  
southwest in the basin. In the lower free troposphere, the high PM<sub>2.5</sub> centers were distributed over the  
northwestern and southwestern SCB areas, as well as the central SCB region. For this event, the regional  
30 emissions from SCB contributed 75.4–94.6 % to the surface PM<sub>2.5</sub> concentrations in SCB. The SCB  
emission export was the major source of the PM<sub>2.5</sub> over the eastern regions of TP and the northern regions



of YGP, with contribution rates of 72.7% and 70.5 %, respectively, during the dissipation stage of heavy air pollution over SCB, which was regarded as the major pollutant sources affecting atmospheric environment changes in Southwest China.

## 35 **1 Introduction**

Haze pollution has brought serious environmental problems, especially in the densely populated and economically developed regions in China, with high-level fine particular matters  $PM_{2.5}$  (particulate matter with an aerodynamically diameter equal to or less than  $2.5 \mu m$ ) (Guo et al., 2014; Li et al., 2015; Gu and Yim, 2016; Lin et al. 2018). Owing to the significant adverse effects on human health and climate  
40 change (Dawson et al., 2007; Langrish et al., 2012; Megaritis et al., 2014; Guo et al., 2016), understanding  $PM_{2.5}$  pollution distributions and mechanisms is of high interest in environmental and climate studies.

Anthropogenic pollutant emissions and stagnant meteorological conditions are commonly regarded as two key factors for haze pollution with excessive concentrations of  $PM_{2.5}$  (Yim et al., 2014; Zhang et  
45 al., 2015; Cai et al., 2017). With strong anthropogenic emissions and favorable meteorological conditions, four main regions with frequent heavy haze pollution are determined, centered over the North China Plain (NCP) (Tao et al., 2012; Ye et al., 2016; Zhang et al., 2016; Huang et al., 2017), the Yangtze River Delta (YRD) in East China (Wang et al., 2012; Li et al., 2015; Tang et al., 2015; Ming et al., 2017), the Pearl River Delta (PRD) in South China (Wu et al., 2013; Zhang et al., 2013; Zhang et al., 2014; Guo et  
50 al., 2016), and the Sichuan Basin (SCB) in Southwest China (Tao et al., 2013; Chen and Xie, 2014; Zhou et al., 2019), respectively. Haze pollution over NCP, YRD and PRD, the main economic centers, with the large flatland has been extensively studied. However, air pollution in the SCB region with high frequent heavy  $PM_{2.5}$  pollution has been insufficiently understood owing to the complex deep basin terrain, in particular the effect of the immediately adjoining Tibetan Plateau (TP).

55 The TP's "harbor effect" on the tropospheric westerlies favors a stable atmospheric stratification and low wind speeds in the boundary layer over the downstream SCB (Xu et al., 2015; Xu et al., 2016), which is conducive to air pollutant accumulation in SCB (Yim et al., 2014; Xu et al., 2016; Wang et al., 2018). The downslope flows at the lee side of the plateau could induce the special stagnation meteorological condition in the lower troposphere (Wang et al., 2015; Ning et al., 2018a). The air-



60 stagnation days account for 76.6 % of the total days in winter over SCB (Liao et al., 2018), where near-  
surface weaken wind, strong vertical air temperature inversion and shallow boundary layer could  
significantly restrain atmospheric diffusion capacity (Ning et al., 2018a; Wang et al., 2018; Tian et al.,  
2019), resulting in the occurrence of heavy air pollution in SCB.

The SCB, covering 260,000 km<sup>2</sup> of Sichuan-Chongqing plain with a dense population of more than  
65 100 million people, is a deep basin surrounded by plateaus and mountains in Southwest China. It is  
immediately to the east of TP with a large elevation drop exceeding 3000 m over a short horizontal  
distance. The unique terrain effect generates the asymmetries of meteorological and air pollutant  
distribution (Zhang et al., 2019), with a remarkable difference of PM<sub>2.5</sub> concentrations between the  
eastern and western regions over SCB (Chen and Xie, 2012; Ning et al., 2018b). The weak vertical  
70 diffusion in the atmospheric boundary layer is one of the main causes for air pollution in winter (Ye et  
al., 2013; Hu et al., 2014; Tian et al., 2017; Zhao et al., 2018). Many evidences suggested that air pollution  
over SCB is mostly caused by the accumulation of air pollutants originating from the local emissions  
(Chen et al., 2014; Liao et al., 2017; Wang et al., 2018; Qiao et al., 2019). However, due to the complex  
flows in SCB, it is important to study how the PM<sub>2.5</sub> is circulated three-dimensionally in order to more  
75 accurately estimate the roles of local emissions and exchanges with outside regions.

In this paper, the observation data analysis and numerical experiments were carried out to analyze  
the three-dimensional distribution of PM<sub>2.5</sub> concentrations in SCB during a heavy haze pollution episode  
in January 2017. The contributions of the SCB pollutant emissions and the PM<sub>2.5</sub> transport to the  
surrounding plateaus and mountains were estimated. Section 2 introduced the observation data and  
80 modeling methods for this study. Section 3 characterized the horizontal and vertical distributions of PM<sub>2.5</sub>  
concentrations during the formation, maintenance and dissipation stages of the heavy haze pollution  
episode. We also assessed the contribution of local emissions to the heavy PM<sub>2.5</sub> pollution within SCB,  
and the impact of external transport of the SCB PM<sub>2.5</sub> to the surrounding areas in Southwest China.  
Summaries and conclusions are provided in Section 4.

## 85 2. Data and model

### 2.1 Observation Data

The surface air pollutant concentrations and meteorological elements observed in 18 cities (Fig. 1;



Table 1) over SCB were used to investigate the distribution of  $PM_{2.5}$ , weather circulations as well as the modeling performance. The hourly meteorological observational data, containing surface air temperature, relative humidity, wind speed and wind direction, were obtained from the Chinese meteorological monitoring network, and the hourly observational  $PM_{2.5}$  concentrations from the China National Environmental Monitoring Center (<http://www.cnemc.cn>).

Besides the above conventional observations, sounding observations were conducted every three hours by using a kite balloon with the sounding system TT12 DigiCORA (Vaisala, Finland) at the Meteorological Observatory of Chengdu (Site 1 in Fig. 1) during 1–20 January 2017. The vertical sounding data of air temperature, wind speed, wind direction and relative humidity were observed at time intervals of 1 second. In addition, a Micro Pulse Lidar Type 4 System (MPL-4B-IDS, Sigma Space, America) was operated at the observational site Ya'an (Site 15 in Fig. 1) in the western SCB edge to retrieve the vertical  $PM_{2.5}$  structures at 532 nm (laser emission wavelength), 2500 Hz (laser repetition rate) and 6–8  $\mu$ J (optimal laser output range).

### 2.3 Model configuration and simulation experiments

The Weather Research and Forecasting with Chemistry (WRF-Chem, version 3.8.1) model was employed to simulate the severe haze pollution event over 2–8 January 2017 in SCB (Fig. 2). A spin-up time of modeling for the first 24 hours starting on 1 January 2017 was dropped. The ERA-Interim meteorological reanalysis data of the European Centre for Medium-Range Weather Forecasts (<https://www.ecmwf.int/en/forecasts/datasets/reanalysis-datasets/>) were served as the initial and boundary conditions of the WRF-Chem simulation. The model domains and the topography were shown in Fig. 1. There were three nesting domains with a domain 1 (D1) covering the most areas of China, a domain 2 (D2) covering Southwest China, and an inner domain 3 (D3) covering SCB and the surrounding areas, at grid intervals of 48, 12 and 3 km respectively (Fig. 1). The physical schemes for the WRF-Chem simulations were listed in Table 2.

The Regional Acid Deposition Model, version 2 (RADM2) (Stockwell et al., 1990) was selected for the atmospheric chemistry mechanism, including the main inorganic ions, elemental carbon, primary and secondary organic aerosol as well as other aerosol species. (Tuccella et al. 2012). The Multi-resolution



115 Emission Inventory for China (MEIC) from 2012 (<http://www.meicmodel.org>) with a horizontal resolution  $0.25 \times 0.25^\circ$  was used for modeling anthropogenic emissions of air pollutants. The vertical turbulent diffusion coefficient of the boundary layer was reduced for modeling the heavy haze pollution according to Wang et al. (2018).

Two simulation experiments were conducted: 1) a baseline simulation (Emi-Real), with the MEIC  
120 anthropogenic emission inventory over all three domains, and 2) a sensitivity simulation (Emi-Non): same as the baseline simulation Emi-Real but shutting down the anthropogenic emission sources in SCB (Fig. 1). By comparing the  $PM_{2.5}$  concentrations between the experiments Emi-Real and Emi-Non, we could quantify the contribution of local emission sources to the heavy haze pollution over SCB and estimate the transport from the polluted SCB to the adjoined areas over the Eastern TP, the northern YGP  
125 and the Daba Mountain (DBM) region (Fig. 1).

#### 2.4 Case description

A severe haze pollution event occurred during 2–8 January 2017 in SCB. As shown in Fig. 2, high and low  $PM_{2.5}$  concentrations were centered respectively in the western and eastern regions during the episode, presenting a generally asymmetric horizontal distribution.

130 Based on the National Ambient Air Quality Standards of China by the Ministry of Ecology and Environment in 2012 (<http://www.mee.gov.cn/>), light and heavy air pollution levels of  $PM_{2.5}$  are categorized with daily average  $PM_{2.5}$  concentrations exceeding 75 and 150  $\mu\text{g m}^{-3}$  in ambient air, respectively. The most heavily polluted region was mainly concentrated in the northwestern city cluster of SCB, including Chengdu, Deyang and Meishan, with the daily mean concentrations of  $PM_{2.5}$   
135 exceeding 150  $\mu\text{g m}^{-3}$  (Figs. 1 and 2a). An hourly  $PM_{2.5}$  peak of 345.0  $\mu\text{g m}^{-3}$  was observed in Chengdu, a representative megacity in Southwest China. According to the hourly  $PM_{2.5}$  variations in the city cluster over the northwestern SCB region, we divided the heavy haze episode into three periods P1, P2 and P3, respectively for formation (from 12:00 p.m. on 2 January to 0:00 on 5 January 2017), maintenance (from 0:00 a.m. on 5 January to 12:00 p.m. on 6 January 2017) and dissipation (from 12:00 p.m. on 6 January  
140 0:00 a.m. on 6 January 2017) stages (local time was used in this study). As shown in Fig. 2b, during P1, the surface  $PM_{2.5}$  concentrations sharply increased to the heavy haze pollution level, and then it fluctuated at the heavy pollution level in P2. Finally in P3, the concentrations of  $PM_{2.5}$  dropped below 75  $\mu\text{g m}^{-3}$



and ended on 8 January 2017 (Fig. 2b).

Analysis of the observations found noteworthy patterns of spatial distribution of surface  $PM_{2.5}$  concentrations over SCB in the formation, maintenance and dissipation periods (Fig. 3). During P1, the surface  $PM_{2.5}$  concentrations were distributed relatively even over SCB, but in the maintenance period P2, the  $PM_{2.5}$  concentrations exhibited a northeast-southwest gradient and a dramatic increase in the western SCB area. For example, the surface  $PM_{2.5}$  concentrations increased from 202.1 to 276.6  $\mu\text{g m}^{-3}$ , from 148.6 to 181.0  $\mu\text{g m}^{-3}$ , from 104.9 to 205.7  $\mu\text{g m}^{-3}$ , and from 145.6 to 168.4  $\mu\text{g m}^{-3}$  respectively, at sites 1, 3, 6 and 15 (Fig. 1; Table 1). In contrast, during the dissipation period P3, strong northeasterly winds developed and the air quality was improved from the northeast to the southwest regions, with  $PM_{2.5}$  cleaned up in the northeastern SCB (Fig. 3). The northeast-southwest gradients of the surface  $PM_{2.5}$  concentrations in SCB were mostly resulted from the near-surface northeasterly winds that were blocked by plateaus and mountains located to the southwest of SCB, which will be further discussed in the following sections.

### 3. Results and discussion

#### 3.1 Model evaluation

We first validated the WRF-Chem simulation performance. The simulation results are compared with the meteorological and  $PM_{2.5}$  observations in SCB, including the intensive vertical soundings for verifying the vertical structures of the simulated boundary layer. The simulated vertical  $PM_{2.5}$  distribution in the lower troposphere was evaluated with the ground-based MPL detection at site 15 at the western SCB (Fig. 1, Table 1).

The reasonable simulation of meteorology is crucial for modeling air pollutant changes (Hanna et al., 2001). The meteorological simulation was validated by comparing with hourly surface meteorological observations of 2 m air temperature (T2), 10 m wind speed (WS10) and relative humidity (RH). The statistical metrics of comparisons between simulated and observed meteorological variables were given in Table 3, including the mean bias (MB), the mean error (ME) and the root mean squared error (RMSE). The verification metrics show a reasonable good model performance with a reference to the previous works (Emery et al., 2001; Chang and Hanna, 2004), although RH was a bit underestimated and wind speed was slightly overestimated. Furthermore, the statistical verification of the simulated



surface  $\text{PM}_{2.5}$  concentrations were shown in Table 4 with the normalized mean bias (NMB), the normalized mean error (NME), the mean fractional bias (MFB) and the mean fractional error (MFE) in two levels of light  $\text{PM}_{2.5}$  pollution ( $75\text{--}150\ \mu\text{g m}^{-3}$ ) and heavy  $\text{PM}_{2.5}$  pollution ( $> 150\ \mu\text{g m}^{-3}$ ). In general, the verification suggested that the WRF-Chem simulations reasonably reproduced the meteorological  
175 conditions and the evolution of  $\text{PM}_{2.5}$  concentrations over SCB, within the criteria for regulatory applications (Emery et al. 2017).

The vertical structure of the atmospheric boundary layer directly affects the vertical diffusion of atmospheric pollutants. Therefore, we compared the vertical profiles of the model simulation with the intensive sounding observations in terms of variation range and average profiles during the heavy haze  
180 episode. The potential temperature, wind speed and relative humidity of the simulation were validated for both daytime and nighttime in Fig. 4. The simulated vertical profiles of meteorological variables were generally acceptable in the lower troposphere (Fig. 4). It should be pointed out that the significant underestimation of RH above 1 km, where the observed RH reached nearly 100%, was caused by the clouds due to the abundant moisture at night, that the model failed to reproduce.

185 The MPL-4B lidar, located at site 15 (Fig. 1) in the western edge of SCB to the east of TP, continuously detected aerosol extinction ratios in the troposphere. The vertical distribution of  $\text{PM}_{2.5}$  mass concentrations were derived from the extinction ratio (Ansmann et al., 2012; Córdoba-Jabonero et al., 2016). The height-time cross-section of derived and simulated  $\text{PM}_{2.5}$  mass concentrations from 7:00 a.m. to 2:00 p.m. on 5 January 2017 were presented in Fig. 5. It can be seen that a good agreement between  
190 the lidar observation and the WRF-Chem simulation was achieved. One of the significant features is that besides the occurrence of near-surface high  $\text{PM}_{2.5}$ , which is typical for most heavy haze pollution over the areas with relatively flat terrain, a layer of high  $\text{PM}_{2.5}$  concentrations was developed between 1 and 2 km above ground level (Fig. 5a), leaving a hollow layer between the two heavy polluted layers. The upper high  $\text{PM}_{2.5}$  layer was built with uplifting and then overturning of the air flows associated with the  
195 blocking effect of the TP terrain, which will be addressed in the next section.

### 3.2 Surface $\text{PM}_{2.5}$ concentrations

Figure 6 showed the simulated surface  $\text{PM}_{2.5}$  concentrations and near-surface wind fields during the formation, maintenance and dissipation periods of 2–8 January 2017. The high  $\text{PM}_{2.5}$  concentrations were mostly centered in the northwest and southern SCB regions, featuring the Chengdu-Chongqing



200 urban agglomeration (Fig. 1). From the formation to the maintenance and the dissipation periods, the prevailing northeasterly winds strengthened gradually over SCB (Fig. 6). The high plateaus and mountains, especially YGP and TP to the west of SCB blocked the upcoming northeasterly winds. The spatial distribution of surface  $\text{PM}_{2.5}$  concentrations (Fig. 6) clearly reflects the combined effect of the urban anthropogenic air pollutant emissions and the  $\text{PM}_{2.5}$  accumulations by the flow convergence forced  
205 by the TP and the YGP blocking to prevailing winds. During the formation and maintenance stage, the surface winds were weak ( $1.4\text{--}1.7\text{ m s}^{-1}$ ) over SCB, which was insufficient to dispel the air pollutants, but to continuously accumulate  $\text{PM}_{2.5}$  locally from light to heavy pollution conditions (Fig. 6a, Fig. 6b). In the maintenance period, heavy air pollution blanketed a large area in SCB with excessive  $\text{PM}_{2.5}$  concentrations (mostly  $>150.0\text{ }\mu\text{g m}^{-3}$ ). By the dissipation period, the northeasterly winds intensified and  
210 removed  $\text{PM}_{2.5}$  from SCB (Fig. 6c).

### 3.3 Vertical structures of $\text{PM}_{2.5}$ concentrations

The high terrain of YGP and TP blocked the northeastern airflows over SCB by lifting the airflow along with air pollutants, altering the vertical  $\text{PM}_{2.5}$  distribution. Therefore, it was of great interest to analyze the vertical distribution and the transport structures of  $\text{PM}_{2.5}$  over SCB and the surrounding  
215 regions.

To examine the vertical structures of  $\text{PM}_{2.5}$  concentrations over SCB, we selected the urban site 1 ( $104.02^\circ\text{ E}$ ;  $30.67^\circ\text{ N}$ ) in Chengdu (cf. Fig. 1) as a reference point to investigate the distributions of  $\text{PM}_{2.5}$  and the atmospheric circulations respectively in the vertical-meridional and vertical-zonal cross-sections. The circulation evolutions from a clean environment (Figs. 7a and 8a), and the formation (Figs. 7b and  
220 8b), maintenance (Figs. 7c and 8c) and dissipation periods (Figs. 7d and 8d) of the heavy haze pollution episode were plotted. A remarkable feature in the vertical distributions of  $\text{PM}_{2.5}$  was the unique hollows over SCB, between the high surface concentration and a high  $\text{PM}_{2.5}$  layers at heights of  $1.5\text{--}3\text{ km}$ . The  $\text{PM}_{2.5}$  distribution was developed by the interaction of atmospheric circulations in the free troposphere and topographic effects on the air flows in the boundary layer over SCB (Figs. 7 and 8). Leaside vortices  
225 often occur over SCB due to the effect of the large TP topography on the mid-latitude westerlies in the free troposphere (Zhang et al., 2019). The lee vortex with a strong temperature inversion can act as a lid covering air pollutants within the atmospheric boundary layer over the SCB region (Ning et al. 2018a). In the current case, the lee vortex circulation, working together with the basin near-surface flows, drove





a 3D  $PM_{2.5}$  transport and its temporal changes over SCB (Figs. 7–8).

230 Comparing the vertical structures of  $PM_{2.5}$  and the circulations in different periods, the so-called lid of vortex circulation with the underlying high  $PM_{2.5}$  layers in the uphill near-surface airflows was elevated to the free troposphere in the clean environment and the dissipation periods of the heavy air pollution (Figs. 7a, 7d, 8a and 8d), while the lid with southwesterly wind in vortex circulation was pressed down in the formation and maintenance periods with confining the strong vertical sub-circulations along  
235 the eastern TP upslope to the atmospheric boundary layer (Figs. 7b, 7c, 8b and 8c).

Driven by the near-surface northeasterly winds (Fig. 6), the near-ground airflows with high  $PM_{2.5}$  concentrations over SCB were uplifted respectively over the windward slopes of TP and YGP. And the uphill airflows were restrained and overturned at heights of 1.5–3 km (a.s.l.), forming a vertical sub-circulation over the SCB region, especially the well structured vertical circulations in the formation and  
240 maintenance stages of the heavy air pollution (Figs. 7–8). Governed by the vertical sub-circulations, the downward transport from the high  $PM_{2.5}$  layers could replenish the surface  $PM_{2.5}$  concentrations in the northwest SCB with the addition of near-surface accumulation of air pollutants (Figs. 7b–7c, 8b–8c).

The TP and YGP lee vortex over SCB also modifies the vertical thermo-dynamical structures in the atmosphere (Xu et al., 2016), altering the height and intensity of the lid in stable stratification covering  
245 air pollutants (Ning et al. 2018a). From the formation to maintenance periods of heavy air pollution, accompanying the lowering stable layer in the free troposphere, the uplifted airflows along the windward slopes of TP and YGP were enhanced, and the high  $PM_{2.5}$  layers were restricted at the lower altitudes of 1.5–3.0 km, where the vertical structure of  $PM_{2.5}$  over SCB was characterized with a remarkable hollow sandwiched by a high  $PM_{2.5}$  layers at heights of 1.5–3 km and the highly polluted near-surface layer (Figs.  
250 7b–7c, 8b–8c). In the dissipation period, the aloft high  $PM_{2.5}$  concentrations over SCB were transported to the downwind regions following the airflows in the lower troposphere, as the lid in the southwest region was weakening and elevated into the free troposphere (Figs. 7d and 8d).

### 3.4 Distribution of $PM_{2.5}$ in upper high concentration layer

This section examined the characteristics of the upper-layer high  $PM_{2.5}$  concentrations. The  $PM_{2.5}$   
255 concentrations were averaged between the heights of 1.5–2.5 km and shown in Fig. 9. Comparing with the surface  $PM_{2.5}$  concentrations, the  $PM_{2.5}$  concentrations decreased significantly in the lower free troposphere (Figs. 6 and 9), reflecting an important role of surface air pollutant emissions in the



atmospheric environment over SCB. During the formation period of heavy air pollution event, the  $PM_{2.5}$  particles in the free troposphere were concentrated in the northwestern SCB (Fig. 9a); In the maintenance  
260 period, the high  $PM_{2.5}$  centers were developed in the northwestern SCB edge, and  $PM_{2.5}$  concentrations increased obviously in the southwestern and central SCB regions (Fig. 9b), reflecting the strong vertical diffusion of  $PM_{2.5}$  in the lower troposphere during the heavy air pollution (Figs. 7c and 8c). Driven by strong northeasterly winds in the dissipation period (Fig. 6c), the high  $PM_{2.5}$  concentrations in the lower free troposphere were centered in the narrow southwestern and southern SCB areas (Fig. 9c), where the  
265  $PM_{2.5}$  from the polluted SCB region were transported out at the gap between the eastern TP and northern YGP edge.

### 3.5 Contribution of local emission and outflow transport

Local emission and regional transport of air pollutants are two key factors affecting air quality. Haze pollution events with extremely high  $PM_{2.5}$  concentrations over SCB are ascribed to the accumulation of  
270 local anthropogenic emissions and air pollutant transport over the basin (Wang et al., 2018; Qiao et al., 2019; Zhao et al., 2019). Here, the differences of the  $PM_{2.5}$  concentration between the numerical experiments, Emi-Real and Emi-Non, were analyzed to assess the contribution of regional air pollutant emissions to surface  $PM_{2.5}$  concentrations in SCB and the impact of  $PM_{2.5}$  transport from SCB to the surrounding plateaus and mountains.

275 Figure 10 showed the  $PM_{2.5}$  concentrations emitted from the regional air pollutant sources over the SCB region and the relative contribution rates to air pollution changes. The SCB's regional air pollutant emissions provided surface  $PM_{2.5}$  concentrations from 40.6 to 136.2  $\mu\text{g m}^{-3}$ , contributing 75.4–94.6 % of surface  $PM_{2.5}$  concentrations for the heavy pollution episode over SCB, indicating its dominant role over this isolated deep basin in Southwest China. The regionally emitting  $PM_{2.5}$  concentrations averaged over  
280 SCB were 88.64, 91.04 and 65.96  $\mu\text{g m}^{-3}$  for the formation, maintenance and dissipation periods, respectively. However, it was interesting to point out that the averaged contribution rates of regional air pollutant emissions to surface  $PM_{2.5}$  concentrations in SCB were actually dropped down from 90.7 % in the formation period, 85.6 % in the maintenance period to 83.3 % in the dissipation period (Fig. 10). We think the exchanges of  $PM_{2.5}$  between the polluted air over SCB and the cleaner environment air over the  
285 surrounding plateaus and mountains in Southwest China play a role in this process. (Figs. 7 and 8).

To assess the impact of the  $PM_{2.5}$  transport from SCB on the air quality over the surrounding areas



in Southwest China, we calculated the  $PM_{2.5}$  contribution amounts and rates of SCB's regional air pollutant emissions to the adjoining regions in the plateaus and mountains based on the differences of the  $PM_{2.5}$  concentrations between Emi-real and Emi-Non (Table 5). The near-surface prevailing  
290 northeasterly winds of SCB brought  $PM_{2.5}$  from SCB to the eastern TP edge, the northern YGP edge and the DBM region (Fig. 6), resulting in importing concentrations of surface  $PM_{2.5}$  averaged respectively with 18.0, 31.3 and  $10.4 \mu\text{g m}^{-3}$  during the heavy haze pollution (Table 5). TP and YGP, as clean regions in China (Song et al., 2017; Zhan et al., 2018), were remarkably polluted by the  $PM_{2.5}$  transport from SCB. During the dissipation period of the heavy air pollution episode, the eastern TP edge and northern  
295 YGP regions gained peak imports of  $PM_{2.5}$  at 22.9 and  $41.9 \mu\text{g m}^{-3}$  (Table 5). Thus in this case, the downwind adjoining TP and YGP regions is the main receptor area of the SCB emissions.

Finally, the  $PM_{2.5}$  contribution rates, i.e., the percentages between the  $PM_{2.5}$  concentrations transported from the basin to those in the adjacent regions of plateaus and mountains were calculated for different periods of the heavy  $PM_{2.5}$  pollution over SCB. The surface  $PM_{2.5}$  in the eastern TP edge were  
300 mostly originated from the source region of SCB, with the dominant contribution rates respectively of 63.6, 67.4 and 72.7 % in the formation, maintenance and dispersion periods. The  $PM_{2.5}$  import from the SCB pollutant emissions also contributed the majority of surface  $PM_{2.5}$  concentrations in the northern YGP, with contribution rates of 58.3, 52.8 and 70.5 % during three different periods with an overall contribution rate of 58.5 % averaged for the whole SCB heavy air pollution period. In contrast, the DBM  
305 region was less influenced by the SCB's emission sources with a contribution rate of 31.0 % averaged during the heavy air pollution event.

#### 4. Conclusions

By using the multiple ground observations, meteorological sounding data and Micro Pulse Lidar retrievals as well as conducting modeling experiments with the WRF-Chem model, this study  
310 investigated the three-dimensional structures and the development mechanisms of the  $PM_{2.5}$  for a wintertime heavy haze pollution episode over SCB, an isolated deep basin in Southwest China. The roles of the basin pollutant emission and the unique basin circulations were evaluated for their contributions to the 3D distribution of  $PM_{2.5}$  over SCB and to the neighboring YGP, TP, and DMB regions.

The vertical structure of the  $PM_{2.5}$  in the lower troposphere over SCB was characterized with unique  
315 hollows located between a high  $PM_{2.5}$  layer at heights of 1.5–3 km and the high  $PM_{2.5}$  surface layer. It is



found that the hollow was developed by the interaction of the upper-level free tropospheric circulations and lower-level topographic boundary layer. The southwesterlies passed over the TP and YGP resulted in a lee vortex over SCB, which helped form and maintain heavy  $PM_{2.5}$  pollution, with well-developed vertical secondary circulations along the eastern TP upslope, while the southwesterlies with the underlying high  $PM_{2.5}$  layers were elevated in the dissipation of heavy  $PM_{2.5}$  pollution over the SCB.

Due to the effect of the joint impact of the urban anthropogenic air pollutant emissions and the large terrain blocking flow at the eastern TP slope and YGP, high surface  $PM_{2.5}$  concentrations were mostly distributed in the northwest and southern SCB regions. The tropospheric circulations with altering the vertical diffusion of  $PM_{2.5}$  exerted a strong impact on  $PM_{2.5}$  distribution in the lower free troposphere. The high  $PM_{2.5}$  centers in the lower free troposphere were distributed over the northwestern and southwestern SCB edges, as well as the central SCB regions. Driven by strong northeasterly winds in the dissipation period, the  $PM_{2.5}$  in the lower free troposphere were converged to the west boundary of SCB and then transported to the eastern TP edge and the northern YGP edge areas.

The regional emissions of air pollutants in SCB played a dominant role in the formation of the heavy air pollution, contributing 75.4–94.6 % to surface  $PM_{2.5}$  concentrations over the basin for the heavy pollution episode studied herein. Furthermore, the surface  $PM_{2.5}$  concentrations in the eastern TP were mostly transported from the SCB's emission sources, with contribution rates of 63.6, 67.4 and 72.7 % for the formation, maintenance and dispersion periods. Similarly, the SCB also contributed the majority of surface  $PM_{2.5}$  concentrations in the adjacent northern YGP, with an average contribution rate of 58.5 % for the whole SCB pollution period and a very high contribution of 70.5 % during the dissipation period. Therefore, the SCB region is the major air pollutant source for the downwind receptor areas over the adjoining TP and YGP regions and affects the atmospheric environment changes in Southwest China.

This work exposed the unique and important three-dimensional structures of  $PM_{2.5}$  and investigated their formation mechanisms and downwind outflow transport over SCB. The deep basin terrain along with the TP and YGP forcing effect creates very complex  $PM_{2.5}$  pollution conditions over the SCB region, which is dramatically different from those over relatively flat regions. To generalize our findings, further work with more case studies and regional climatic analyses with long-term observation data and numerical modeling with data assimilation and refined physical and chemical schemes are desired. Furthermore, as pointed out in this study, the  $PM_{2.5}$  emission sources in SCB greatly influence the regional environmental changes over Southwest China. Thus, the regional transport modeling of air



pollutants with careful consideration of the thermal and dynamic forcing of underlying complex plateaus terrain should be further investigated.

*Data availability.* Data used in this paper can be provided by Zhuozhi Shu (shuzhuozhi@foxmail.com) upon request.

*Author contributions.* ZS and TZ conducted the study design. ZS, TZ, JX, CW and LC conducted the vertical observational experiment. ZS wrote the manuscript with the help of TZ and YL. LZ and YZ assisted with data processing. HL and LS were involved in the scientific interpretation and discussion. LL and YL provided the surface meteorological data. All of the authors provided commentary on the paper.

*Competing interests.* The authors declare that they have no conflicts of interest.

*Acknowledgements.* This research was supported by the Second Tibetan Plateau Scientific Expedition and Research (STEP) program (2019QZKK0105), the National Natural Science Foundation of China (91744209, 91644223 and 91544109), the National Key R & D Program Pilot Projects of China (2016YFC0203304) and Graduate Research and Innovation Projects of Jiangsu Province (SJKE19\_0941).

## References

- Ansmann, A., Seifert, P., Tesche, M., and Wandinger, U.: Profiling of fine and coarse particle mass: case studies of Saharan dust and Eyjafjallajökull/Grimsvötn volcanic plumes, *Atmos. Chem. Phys.*, 12, 9399–9415, <https://doi.org/10.5194/acp-12-9399-2012>, 2012.
- Cai, W., Li, K., Liao, H., Wang, H. and Wu, L.: Weather conditions conducive to Beijing severe haze more frequent under climate change, *Nat. Clim. Change*, 7, 257–262, <https://doi.org/10.1038/nclimate3249>, 2017.
- Chang, J. C. and Hanna, S. R.: Air quality model performance evaluation, *Meteorol. Atmos. Phys.*, 87, 167–196, <https://doi.org/10.1007/s00703-003-0070-7>, 2004.



- Chen, Y. and Xie, S.: Temporal and spatial visibility trends in the Sichuan Basin, China, 1973 to 2010,  
375 *Atmos. Res.*, 112, 25–34, <https://doi.org/10.1016/j.atmosres.2012.04.009>, 2012.
- Chen, Y., Xie, S., Luo, B. and Zhai, C.: Characteristics and origins of carbonaceous aerosol in the Sichuan  
Basin, China, *Atmos. Environ.*, 94, 215–223, <https://doi.org/10.1016/j.atmosenv.2014.05.037>, 2014.
- Córdoba-Jabonero, C., Andrey-Andrés, J., Gómez, L., Adame, J.A., Sorribas, M., Navarro-Comas, M.,  
Puentedura, O., Cuevas, E., and Gil-Ojeda, M.: Vertical mass impact and features of Saharan dust  
380 intrusions derived from ground-based remote sensing in synergy with airborne in-situ measurements,  
*Atmos. Environ.*, 142, 420–429, <https://doi.org/10.1016/j.atmosenv.2016.08.003>, 2016.
- Dawson, J. P., Adams, P. J., and Pandis, S. N.: Sensitivity of PM<sub>2.5</sub> to climate in the Eastern US: a  
modeling case study, *Atmos. Chem. Phys.*, 7, 4295–4309, <https://doi.org/10.5194/acp-7-4295-2007>,  
2007.
- 385 Emery, C. A., Tai, E., and Yarwood, G.: Enhanced meteorological modeling and performance evaluation  
for two Texas ozone episodes, Project Report prepared for the Texas Natural Resource Conservation  
Commissions, ENVIRON International Corporation, Novato, CA, 2001.
- Emery, C., Liu, Z., Russell, A. G., Odman, M. T., Yarwood, G. and Kumar, N.: Recommendations on  
statistics and benchmarks to assess photochemical model performance, *J. Air. Waste. Manage.*, 67, 582–  
390 598, <https://doi.org/10.1080/10962247.2016.1265027>, 2017.
- Gu, Y. and Yim, S. H.: The air quality and health impacts of domestic trans-boundary pollution in various  
regions of China, *Environ. Int.*, 97, 117–124, <https://doi.org/10.1016/j.envint.2016.08.004>, 2016.
- Guo, S., Hu, M., Zamora, M. L., Peng, J., Shang, D., Zheng, J., Du, Z., Wu, Z., Shao, M., Zeng, L. Molina,  
M. J. and Zhang, R.: Elucidating severe urban haze formation in China, *P. Natl. Acad. Sci. USA.*, 111,  
395 17373–17378, <https://doi.org/10.1073/pnas.1419604111>, 2014.
- Guo, Y., Zeng, H., Zheng, R., Li, S., Barnett, A. G., Zhang, S., Zou, X., Huxley, R., Chen, W. and  
Williams, G.: The association between lung cancer incidence and ambient air pollution in China: a  
spatiotemporal analysis, *Environ. Res.*, 144, 60–65, <https://doi.org/10.1016/j.envres.2015.11.004>, 2016.
- Hanna, S. R. and Yang, R.: Evaluations of mesoscale models' simulations of near-surface winds,  
400 temperature gradients, and mixing depths, *J. Appl. Meteorol.*, 40, 1095–1104,  
[https://doi.org/10.1175/1520-0450\(2001\)040<1095:EOMMSO>2.0.CO;2](https://doi.org/10.1175/1520-0450(2001)040<1095:EOMMSO>2.0.CO;2), 2001.
- Huang, X., Liu, Z., Liu, J., Hu, B., Wen, T., Tang, G., Zhang, J., Wu, F., Ji, D., Wang, L., and Wang, Y.:  
Chemical characterization and source identification of PM<sub>2.5</sub> at multiple sites in the Beijing–Tianjin–



- Hebei region, China, *Atmos. Chem. Phys.*, 17, 12941–12962, [https://doi.org/10.5194/acp-17-12941-](https://doi.org/10.5194/acp-17-12941-2017)  
405 [2017](https://doi.org/10.5194/acp-17-12941-2017), 2017.
- Hu, X., Ma, Z., Lin, W., Zhang, H., Hu, J., Wang, Y., Xu, X., Fuentes, J. D. and Xue, M.: Impact of the Loess Plateau on the atmospheric boundary layer structure and air quality in the North China Plain: A case study. *Sci. Total. Environ.*, 499, 228–237, <https://doi.org/10.1016/j.scitotenv.2014.08.053>, 2014.
- Langrish, J. P., Li, X., Wang, S., Lee, M. M. Y., Barnes, G. D., Miller, M. R., Cassee, F. R., Boon, N. A.,  
410 Donaldson, K., Li, J., Li, L., Mills, N. L., Newby, D. E. and Jiang, L.: Reducing Personal Exposure to Particular Air Pollution Improves Cardiovascular Health in Patients with Coronary Heart Disease, *Environ. Health Persp.*, 120, 367–372, <https://doi.org/10.1289/ehp.1103898>, 2012.
- Li, B., Zhang, J., Zhao, Y., Yuan, S., Zhao, Q., Shen, G. and Wu, H.: Seasonal variation of urban carbonaceous aerosols in a typical city Nanjing in Yangtze River Delta, China, *Atmos. Environ.*, 106,  
415 223–231, <https://doi.org/10.1016/j.atmosenv.2015.01.064>, 2015.
- Li, P., Xin, J., Wang, Y., Li, G., Pan, X., Wang, S., Cheng, M., Wen, T., Wang, Guang. And Liu, Z.: Association between particulate matter and its chemical constituents of urban air pollution and daily mortality or morbidity in Beijing city, *Environ. Sci. Pollut. R.*, 22, 358–368, <https://doi.org/10.1007/s11356-014-3301-1>, 2015.
- 420 Lin, Y., Zou, J., Yang, W. and Li, C.: A review of recent advances in research on PM<sub>2.5</sub> in China, *Int. J. Environ. Res. Public Health*, 15, 438, <https://doi.org/10.3390/ijerph15030438>, 2018.
- Liao, T., Wang, S., Ai, J., Gui, K., Duan, B., Zhao, Q., Zhang, X., Jiang, W. and Sun, Y.: Heavy pollution episodes, transport pathways and potential sources of PM<sub>2.5</sub>, during the winter of 2013 in Chengdu (China), *Sci. Total. Environ.*, 584, 1056–1065, <https://doi.org/10.1016/j.scitotenv.2017.01.160>, 2017.
- 425 Liao, T., Gui, K., Jiang, W., Wang, S., Wang, B., Zeng, Z., Che, H., Wang, Y. and Sun, Y.: Air stagnation and its impact on air quality during winter in Sichuan and Chongqing, southwestern China, *Sci. Total. Environ.*, 635, 576–585, <https://doi.org/10.1016/j.scitotenv.2018.04.122>, 2018.
- Megaritis, A. G., Fountoukis, C., Charalampidis, P. E., Denier van der Gon, H. A. C., Pilinis, C., and Pandis, S. N.: Linking climate and air quality over Europe: effects of meteorology on PM<sub>2.5</sub>  
430 concentrations, *Atmos. Chem. Phys.*, 14, 10283–10298, <https://doi.org/10.5194/acp-14-10283-2014>, 2014.
- Ming, L., Jin, L., Li, J., Fu, P., Yang, W., Liu, D., Zhang, G., Wang, Z. and Li, X.: PM<sub>2.5</sub> in the Yangtze River Delta, China: Chemical compositions, seasonal variations, and regional pollution events, *Environ.*



- Pollut., 223, 200–212, <https://doi.org/10.1016/j.envpol.2017.01.013>, 2017.
- 435 Ning, G., Wang, S., Yim, S. H. L., Li, J., Hu, Y., Shang, Z., Wang, J., and Wang, J.: Impact of low-pressure systems on winter heavy air pollution in the northwest Sichuan Basin, China, *Atmos. Chem. Phys.*, 18, 13601–13615, <https://doi.org/10.5194/acp-18-13601-2018>, 2018a.
- Ning, G., Wang, S., Ma, M., Ni, C., Shang, Z., Wang, J. and Li, J.: Characteristics of air pollution in different zones of Sichuan Basin, China, *Sci. Total. Environ.*, 612, 975–984,
- 440 <https://doi.org/10.1016/j.scitotenv.2017.08.205>, 2018b.
- Qiao, X., Guo, H., Tang, Y., Wang, P., Deng, W., Zhao, X., Hu, J., Ying, Q., and Zhang, H.: Local and regional contributions to fine particulate matter in the 18 cities of Sichuan Basin, southwestern China, *Atmos. Chem. Phys.*, 19, 5791–5803, <https://doi.org/10.5194/acp-19-5791-2019>, 2019.
- Stockwell, W. R., Middleton, P., Chang, J. S. and Tang, X.: The second generation regional acid
- 445 deposition model chemical mechanism for regional air quality modeling, *J. Geophys. Res. Atmos.*, 95, 16343–16367, <https://doi.org/10.1029/JD095iD10p16343>, 1990.
- Song, C., Wu, L., Xie, Y., He, J., Chen, X., Wang, T., Lin, Y., Jin, T., Wang, A., Liu, Y., Dai, Q., Liu, B., Wang, Y. and Mao, H.: Air pollution in China: status and spatiotemporal variations, *Environ. Pollut.*, 227, 334–347, <https://doi.org/10.1016/j.envpol.2017.04.075>, 2017.
- 450 Tang, L., Yu, H., Ding, A., Zhang, Y., Qin, W., Zhuang, W., Chen, W., Hua, Y. and Yang, X.: Regional contribution to PM<sub>1</sub> pollution during winter haze in Yangtze River Delta, China, *Sci. Total. Environ.*, 541, 161–166, <https://doi.org/10.1016/j.scitotenv.2015.05.058>, 2015.
- Tian, P., Cao, X., Zhang, L., Sun, N., Sun, L., Logan, T., Shi, J., Wang, Y., Ji, Y., Lin, Y., Huang, Z., Zhou, T., Shi, Y., and Zhang, R.: Aerosol vertical distribution and optical properties over China from long-term
- 455 satellite and ground-based remote sensing, *Atmos. Chem. Phys.*, 17, 2509–2523, <https://doi.org/10.5194/acp-17-2509-2017>, 2017.
- Tian, M., Liu, Y., Yang, F., Zhang, L., Peng, C., Chen, Y., Shi, G., Wang, H., Luo, B., Jiang, C., Li, B., Takeda, N. and Koizumi, K.: Increasing importance of nitrate formation for heavy aerosol pollution in two megacities in Sichuan Basin, southwest China, *Environ. Pollut.*, 250, 898–905,
- 460 <https://doi.org/10.1016/j.envpol.2019.04.098>, 2019.
- Tao, J., Zhang, L., Engling, G., Zhang, R., Yang, Y., Cao, J., Zhu, C., Wang, Q. and Luo L.: Chemical composition of PM<sub>2.5</sub> in an urban environment in Chengdu, China: Importance of springtime dust storms and biomass burning, *Atmos. Res.*, 122, 270–283, <https://doi.org/10.1016/j.atmosres.2012.11.004>, 2013.





- Tao, M., Chen, L., Su, L. and Tao, J.: Satellite observation of regional haze pollution over the North  
465 China Plain, *J. Geophys. Res. Atmos.*, 117, D12203, <https://doi.org/10.1029/2012JD017915>, 2012.
- Tuccella, P., Curci, G., Visconti, G., Bessagnet, B., and Menut L., and Park, R. J.: Modeling of gas and  
aerosol with WRF-Chem over Europe: Evaluation and sensitivity study, *J. Geophys. Res. Atmos.*, 117,  
D03303, <https://doi.org/10.1029/2011JD016302>, 2012.
- Wang, H., Peng, Y., Zhang, X., Liu, H., Zhang, M., Che, H., Cheng, Y., and Zheng, Y.: Contributions to  
470 the explosive growth of PM<sub>2.5</sub> mass due to aerosol–radiation feedback and decrease in turbulent diffusion  
during a red alert heavy haze in Beijing–Tianjin–Hebei, China, *Atmos. Chem. Phys.*, 18, 17717–17733,  
<https://doi.org/10.5194/acp-18-17717-2018>, 2018.
- Wang, T., Jiang, F., Deng, J., Shen, Y., Fu, Q., Wang, Q., Fu, Y., Xu, J. and Zhang, D.: Urban air quality  
and regional haze weather forecast for Yangtze River Delta region, *Atmos. Environ.*, 58, 70–83,  
475 <https://doi.org/10.1016/j.atmosenv.2012.01.014>, 2012.
- Wang, Q. and Tan, Z.: Multi-scale topographic control of southwest vortex formation in Tibetan Plateau  
region in an idealized simulation, *J. Geophys. Res. Atmos.*, 119, 543–561,  
<https://doi.org/10.1002/2014JD021898>, 2014.
- Wang, X., Dickinson, R. E., Su, L., Zhou, C. and Wang K.: PM<sub>2.5</sub> pollution in China and how it has been  
480 exacerbated by terrain and meteorological conditions, *Bull. Amer. Meteor. Soc.*, 99, 105–119,  
<https://doi.org/10.1175/BAMS-D-16-0301.1>, 2018.
- Wang, H., Tian, M., Chen, Y., Shi, G., Liu, Y., Yang, F., Zhang, L., Deng, L., Yu, J., Peng, C., and Cao,  
X.: Seasonal characteristics, formation mechanisms and source origins of PM<sub>2.5</sub> in two megacities in  
Sichuan Basin, China, *Atmos. Chem. Phys.*, 18, 865–881, <https://doi.org/10.5194/acp-18-865-2018>,  
485 2018.
- Wu, M., Wu, D., Fan, Q., Wang, B. M., Li, H. W., and Fan, S. J.: Observational studies of the  
meteorological characteristics associated with poor air quality over the Pearl River Delta in China, *Atmos.*  
*Chem. Phys.*, 13, 10755–10766, <https://doi.org/10.5194/acp-13-10755-2013>, 2013.
- Xu, R., Tang, G., Wang, Y. and Tie, X.: Analysis of a long-term measurement of air pollutants (2007–  
490 2011) in North China Plain (NCP); Impact of emission reduction during the Beijing Olympic Games,  
*Chemosphere*, 159, 647–658, <https://doi.org/10.1016/j.chemosphere.2016.06.025>, 2016.
- Xu, X., Wang, Y., Zhao, T., Cheng, X., Meng, Y. and Ding, G.: "Harbor" effect of large topography on  
haze distribution in eastern China and its climate modulation on decadal variations in haze, *Chinese Sci.*



- Bull., 60, 1132–1143, <https://doi.org/10.1360/N972014-00101>, 2015.
- 495 Xu, X., Zhao, T., Liu, F., Gong, S. L., Kristovich, D., Lu, C., Guo, Y., Cheng, X., Wang, Y., and Ding, G.: Climate modulation of the Tibetan Plateau on haze in China, *Atmos. Chem. Phys.*, 16, 1365–1375, <https://doi.org/10.5194/acp-16-1365-2016>, 2016.
- Ye, X., Song, Y., Cai, X. and Zhang, H.: Study on the synoptic flow patterns and boundary layer process of the severe haze events over the North China Plain in January 2013, *Atmos. Environ.*, 124, 129–145, <https://doi.org/10.1016/j.atmosenv.2015.06.011>, 2016.
- 500 Yim, S. H. L., Fung, J. C. H. and Ng, E. Y. Y.: An assessment indicator for air ventilation and pollutant dispersion potential in an urban canopy with complex natural terrain and significant wind variations, *Atmos. Environ.*, 94, 297–306, <https://doi.org/10.1016/j.atmosenv.2014.05.044>, 2014.
- Zhang, Y., Shao, M., Lin, Y., Luan, S., Mao, Ning., Chen, W. and Wang, M.: Emission inventory of carbonaceous pollutants from biomass burning in the Pearl River Delta Region, China, *Atmos. Environ.*, 76, 189–199, <https://doi.org/10.1016/j.atmosenv.2012.05.055>, 2013.
- Zhang, Q., Quan, J., Tie, X., Li, X., Liu, Q., Gao, Y. and Zhao, D.: Effects of meteorology and secondary particle formation on visibility during heavy haze events in Beijing, China, *Sci. Total. Environ.*, 502, 578–584, <https://doi.org/10.1016/j.scitotenv.2014.09.079>, 2015.
- 510 Zhang, Z., Zhang, X., Gong, D., Kim, S.-J., Mao, R., and Zhao, X.: Possible influence of atmospheric circulations on winter haze pollution in the Beijing–Tianjin–Hebei region, northern China, *Atmos. Chem. Phys.*, 16, 561–571, <https://doi.org/10.5194/acp-16-561-2016>, 2016.
- Zhang, L., Guo, X., Zhao, T., Gong, S., Xu, X., Li, Y., Luo, L., Gui, K., Wang, H., Zheng, Y. and Yin, X.: A modelling study of the terrain effects on haze pollution in the Sichuan Basin, *Atmos. Environ.*, 196, 77–85, <https://doi.org/10.1016/j.atmosenv.2018.10.007>, 2019.
- 515 Zhao, S., Yu, Y., Yin, D., Qin, D., He, J. and Dong, L.: Spatial patterns and temporal variations of six criteria air pollutants during 2015 to 2017 in the city clusters of Sichuan Basin, China, *Sci. Total. Environ.*, 624, 540–557, <https://doi.org/10.1016/j.scitotenv.2017.12.172>, 2018.
- Zhao, S., Yu, Y., Qin, D., Yin, D., Dong, L. and He, J.: Analyses of regional pollution and transportation of PM<sub>2.5</sub> and ozone in the city clusters of Sichuan Basin, China, *Atmos. Pollut. Res.*, 10, 374–385, <https://doi.org/10.1016/j.apr.2018.08.014>, 2019.
- 520 Zhan, D., Kwan, M. P., Zhang, W., Yu, X., Meng, B. and Liu, Q.: The driving factors of air quality index in China, *J. Clean Prod.*, 197, 1342–1351, <https://doi.org/10.1016/j.jclepro.2018.06.108>, 2018.



Zhou, Y., Luo, B., Li, J., Hao, Y., Yang, W., Shi, F., Chen, Y., Simayi, M. and Xie, S.: Characteristics of  
525 six criteria air pollutants before, during, and after a severe air pollution episode caused by biomass  
burning in the southern Sichuan Basin, China, Atmos. Environ., 215, 116840,  
<https://doi.org/10.1016/j.atmosenv.2019.116840>, 2019.



530

**Table 1.** Names of 18 observation sites with the corresponding site number (Fig. 1b) in SCB.

Number	1	2	3	4	5	6
Names	Chengdu	Chongqing	Deyang	Guang'an	Leshan	Meishan
Number	7	8	9	10	11	12
Names	Mianyang	Nanchong	Neijiang	Suining	Yibin	Ziyang
Number	13	14	15	16	17	18
Names	Zigong	Luzhou	Ya'an	Bazhong	Dazhou	Guangyuan

535

**Table 2.** Setting of physical schemes in the WRF-Chem simulations

Microphysics	Morrison 2-mom
Boundary layer	MYJ
Longwave radiation	RRTMG
Shortwave radiation	RRTM
Land surface	Noah

540



**Table 3.** The statistical metrics of comparisons between simulated and observed meteorological

545 elements during 2–8 January 2017.

	Obs.	Sim.	R	MB	ME	RMSE
T2	9.9	9.2	0.78**	-0.7	1.7	2.1
RH	85.1	77.7	0.67**	-7.4	11.2	13.4
WS10	1.2	1.5	0.41*	0.3	0.8	1.1

Note: MB, ME, RMSE were calculated as following:  $MB = \frac{1}{N} \sum_{i=1}^N (M_i - O_i)$ ;  $ME = \frac{1}{N} \sum_{i=1}^N |M_i - O_i|$ ;  $RMSE = \sqrt{\frac{1}{N} \sum_{i=1}^N (M_i - O_i)^2}$ ; (M and O represented the results from simulation and observation). The \*\* and \* respectively indicated passing the 99% and 95% significant test.

550

**Table 4.** The statistical metrics of comparisons between simulated and observed surface PM<sub>2.5</sub>

concentrations in two levels of light and heavy PM<sub>2.5</sub> pollution during 2–8 January 2017.

	NMB (%)	NME (%)	MFB (%)	MFE (%)
Light pollution	-4.3	25.4	-7.7	30.0
Heavy pollution	-13.5	33.4	-16.3	37.4

Note: NMB, NME, MFB and MFE were calculated as following:  $NMB = \frac{\sum_{i=1}^N (M_i - O_i)}{\sum_{i=1}^N O_i} \cdot 100\%$ ;

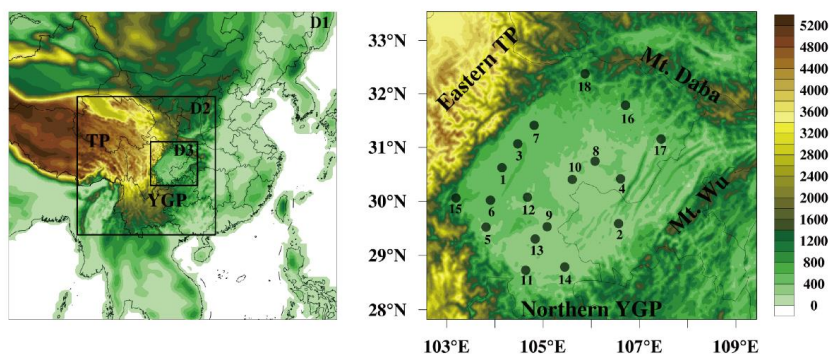
555  $NME = \frac{\sum_{i=1}^N |M_i - O_i|}{\sum_{i=1}^N O_i} \cdot 100\%$ ;  $MFB = \frac{1}{N} (2 \cdot \frac{M_i - O_i}{M_i + O_i}) \cdot 100\%$ ;  $MFE = \sum_{i=1}^N \left| 2 \cdot \frac{M_i - O_i}{M_i + O_i} \right| \cdot 100\%$ .



560

**Table 5.** The amounts and contribution rates of PM<sub>2.5</sub> trans-boundary transport from SCB to surface PM<sub>2.5</sub> concentrations averaged over the eastern TP edge (ETP), northern YGP edge (YGP) and DBM region during the formation (P1), maintenance (P2) and dissipation (P3) periods of the heavy haze pollution episodes over the SCB region.

	Region	P1	P2	P3	Averages
Transport amount ( $\mu\text{g m}^{-3}$ )	ETP	15.4	18.8	22.5	18.0
	YGP	30.1	27.5	41.9	31.3
	DBM	8.6	13.5	8.4	10.4
Contribution rates (%)	ETP	63.6	67.4	72.7	66.6
	YGP	58.3	52.8	70.5	58.5
	DBM	26.7	36.6	30.1	31.0



570 **Figure 1.** (Left panel) three nesting domains D1, D2 and D3 of WRF-Chem simulation with the terrain  
heights (m in a.s.l.) and (right panel) the location of 18 urban observation sites (black dots, Table 1)  
including site 1 (Chengdu) with the intensive sounding observations and site 15 (Ya'an) with the ground-  
based MPL detection in SCB with the surrounding Tibetan Plateau (TP), Yunnan-Guizhou Plateau (YGP),  
Mountains Daba (Mt. Daba) and Wu (Mt. Wu) in Southwest China.

575

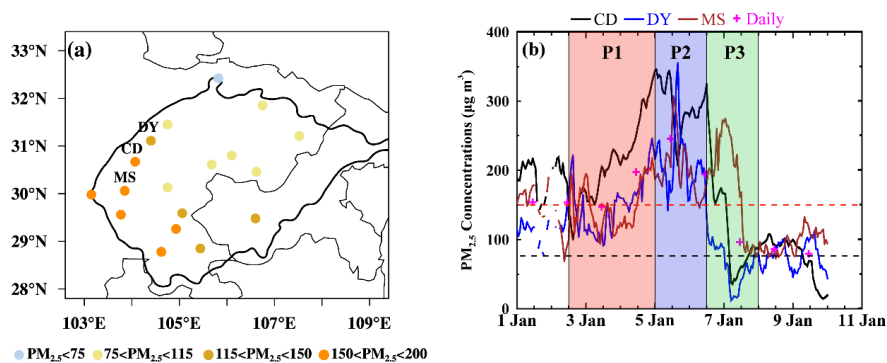


**Figure 2.** (a) Surface  $PM_{2.5}$  concentrations over 18 urban sites averaged during the heavy haze pollution over 2–8 January 2017. (b) hourly variations of  $PM_{2.5}$  concentrations observed at the three heaviest polluted cities Chengdu (CD), Deyang (DY) and Meishan (MS) (Fig. 1; Table 1) over 1–10 January 2017. The P1, P2 and P3 indicated respectively the formation, maintenance and dissipation periods of heavy haze pollution with the light pollution level of  $75 \mu\text{g m}^{-3}$  (black dashed line) and heavy pollution level of  $150 \mu\text{g m}^{-3}$  (red dashed line).





585

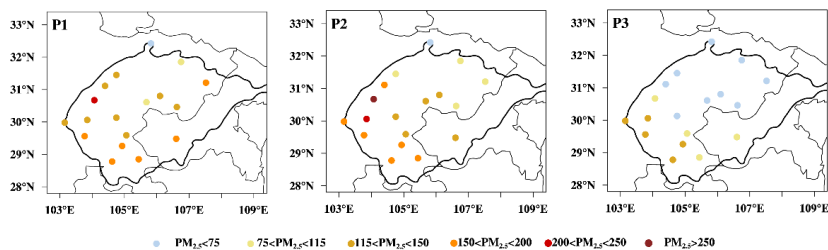


**Figure 3.** The spatial distributions of observed surface  $PM_{2.5}$  concentrations in SCB averaged in the formation, maintenance and dissipation periods P1, P2 and P3 (Fig. 2b) of the heavy haze pollution episode over 2–8 January 2017.

590

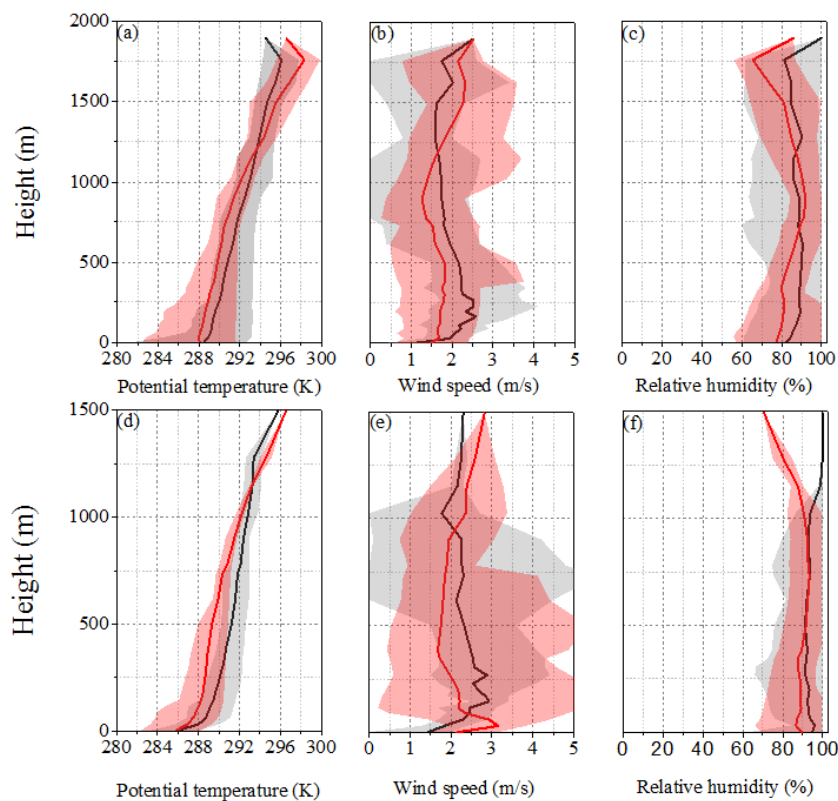


**Figure 4.** The comparisons of observed and simulated vertical profiles of potential temperature, wind speed and relative humidity in the daytime (a, b, c) and nighttime (d, e, f) at Chengdu (site 1 in Fig. 1) during 2-8 January 2017. The red and gray shaded areas represented the variation range of simulation and observation in all vertical profiles with averaged values (lines), respectively.

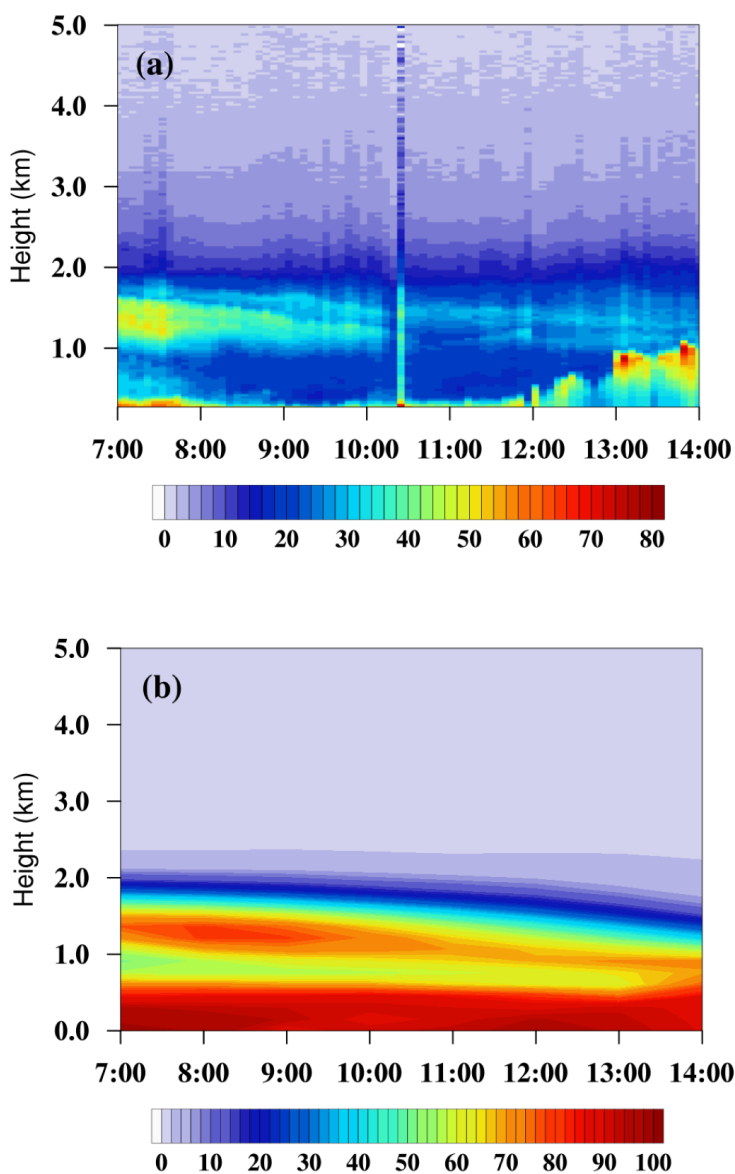


**Figure 5.** Vertical and time cross-sections of PM<sub>2.5</sub> mass concentrations ( $\mu\text{g m}^{-3}$ ) from (a) MPL-4B  
600 retrievals products and (b) simulation results at site 15 (Fig. 1; Table 1) in the western SCB edge during  
7:00 a.m.–2:00 p.m. on 5 January 2017.

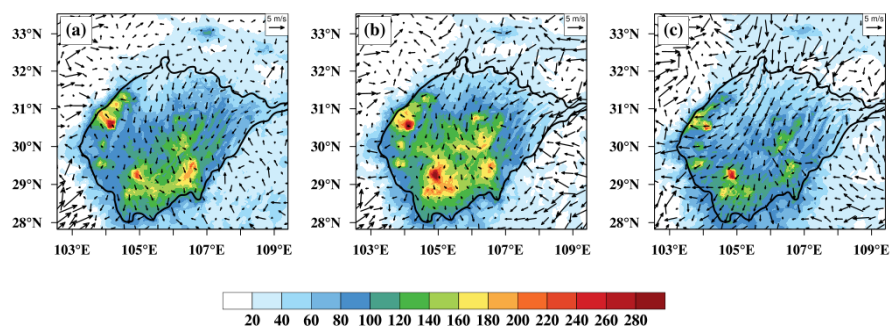


**Figure 6.** Horizontal distribution of surface  $\text{PM}_{2.5}$  concentrations ( $\mu\text{g m}^{-3}$ ; color contours) and wind vectors at 10 m averaged in the periods (a) P1 (b) P2 and (c) P3 respectively. The SCB was outlined with  
605 an altitude contour line of 750 m (a.s.l.; black lines).

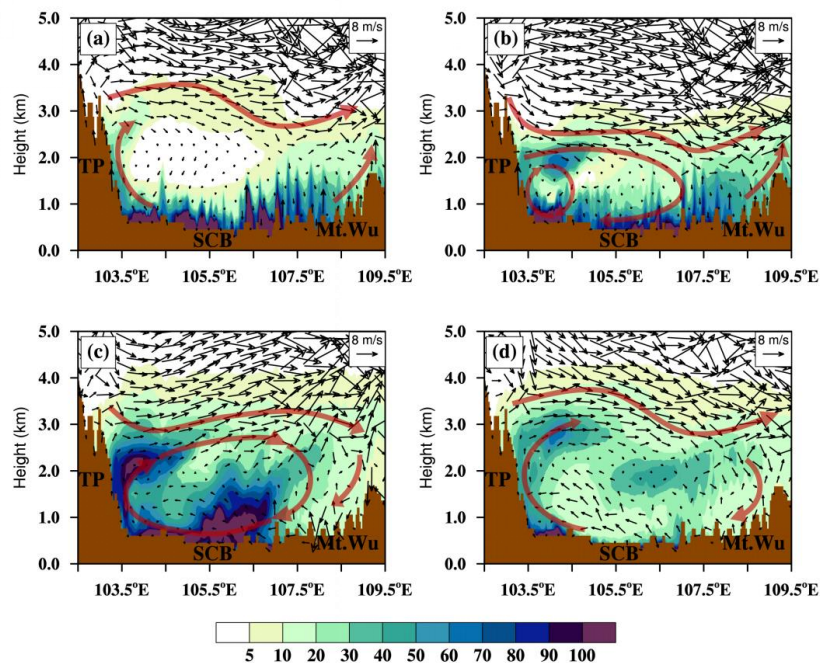
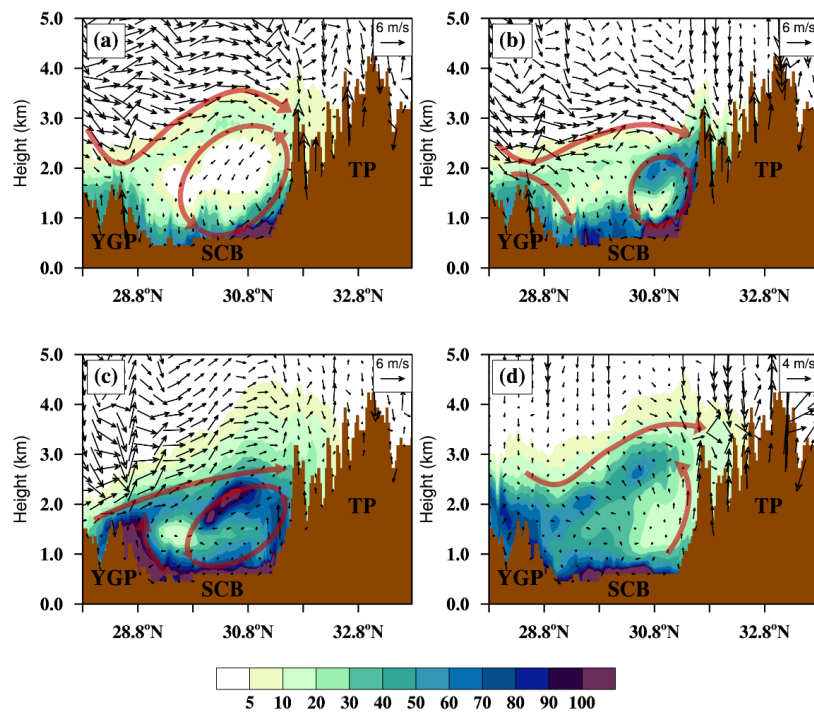
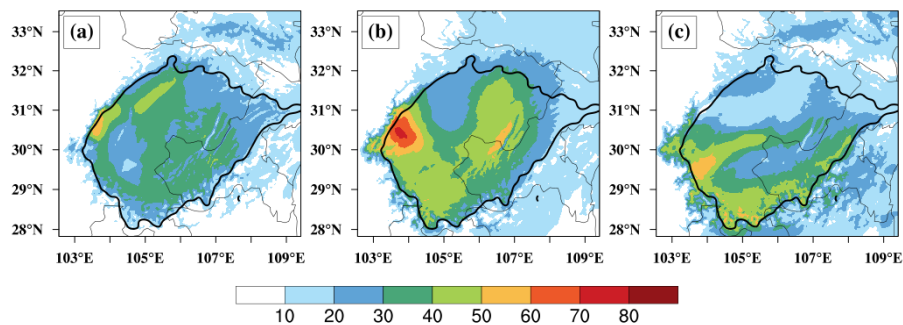


**Figure 7.** Height-longitude cross-sections of  $\text{PM}_{2.5}$  concentrations (color contours:  $\mu\text{g m}^{-3}$ ) and wind  
610 vectors along  $30.67^\circ \text{N}$  in the (a) clean environment at 12:00 a.m. on 2 January 2017 (b) heavy air  
pollution formation stage at 12:00 a.m. on 3 January 2017 (c) maintenance stage at 8:00 a.m. on 6 January  
2017, and (d) dissipation stage at 8:00 a.m. on 7 January 2017. The brown arrows highlighted the major  
air flows (red arrows) associated with the terrain of TP, SCB and Mt. Wu (filled brown color).



615

**Figure 8.** Same as Fig. 7, but for height-latitude cross-sections of  $PM_{2.5}$  concentrations and wind vectors.



620 **Figure 9.** Horizontal distribution of  $\text{PM}_{2.5}$  concentrations (color contours:  $\mu\text{g m}^{-3}$ ) averaged between 1.5 and 2.5 km heights (in the lower free troposphere) for (a) formation, (b) maintenance and (c) dissipation periods of heavy haze pollution episode over SCB. The SCB was outlined with an altitude contours of 750 m in a.s.l. (dark black lines).



625

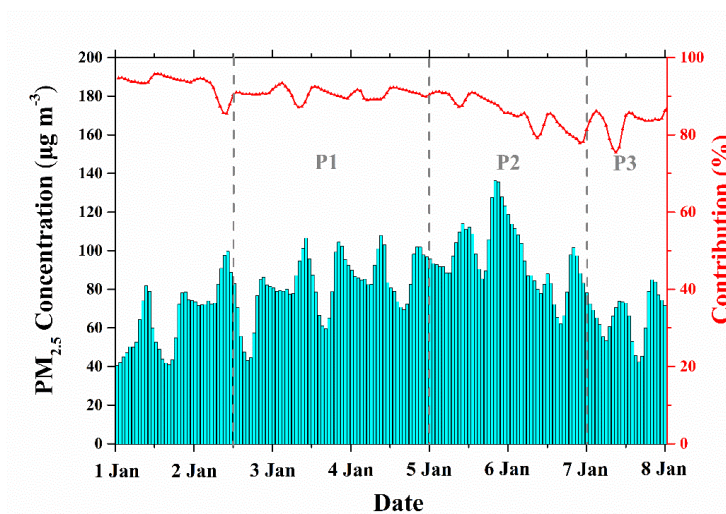


**Figure 10.** Hourly variations of surface  $\text{PM}_{2.5}$  concentrations emitted from the SCB's regional anthropogenic emission sources (blue filled areas) and the contribution proportions to the basin-region surface  $\text{PM}_{2.5}$  levels (red curve) during 1–8 January 2017.

630